Fe_3O_4-loaded Ion Exchange Resin for Chromatographic Separation of Boron Isotopes: Experiment and Numerical Simulation

Qingfeng Wang[1,2], Tao Chen[1,2], Peng Bai[1,2], Jiafei Lyu[1,2,*], Xianghai Guo[1,2,3,*]

[1]*School of Chemical Engineering and Technology, Tianjin University, Tianjin 300350, P. R. China*

[2]*Key Laboratory of Systems Bioengineering, Ministry of Education, Tianjin University, Tianjin, 300072, P. R. China*

[3]*School of Marine Science and Technology, Tianjin University, Tianjin 300072, P. R. China*

*Corresponding author E-mail: guoxh@tju.edu.cn (X. Guo)

jflv@tju.edu.cn (J. Lyu)

ABSTRACT

Fe_3O_4-loaded ion exchange resin composites (Fe_3O_4@Resin) were optimally constructed through ion exchange and co-precipitation of Fe^{2+} and Fe^{3+} on strong acid ion exchange resin. The as-synthesized Fe_3O_4@Resin composite was sophisticatedly characterized and investigated for $^{10}B/^{11}B$ separation including effect of *p*H, kinetics and isotherms through batch adsorption experiments which can be well described by pseudo-second order kinetics and Langmuir model. In the chromatographic column packed with Fe_3O_4@Resin, ^{10}B was selectively retained with a high dynamic separation factor of 1.312. Considering the consistency between simulated and experimental breakthrough curves within Fe_3O_4@Resin packed column, chromatographic $^{10}B/^{11}B$ separation performance was simulated under various conditions which were further optimized by Box-Behnken design. Consequently, the annual yield of ^{10}B reached the maximum of 612 g with feed concentration of 7.567 $g \cdot L^{-1}$, flow rate of 38.57 $mL \cdot min^{-1}$, and column size of 2.2×45 cm (I.D. × length). In addition, five-cycle adsorption/regeneration experiments demonstrated its merit of reusability.

Topical heading: Separations: Materials, Devices and Processes

Keywords: boron isotopic separation, Fe_3O_4-loaded ion exchange resin, chromatographic column, process optimization, industrial application

1. INTRODUCTION

As an important raw material, boron has been widely used in ceramics, semiconductors, superconductors and metallurgical industries[1]. ^{10}B and ^{11}B, as stable boron isotopes with natural abundance of 80.2% and 19.8%, have individual applications due to their distinct neutron absorption properties. Large thermal neutrons absorption cross-sections of ^{10}B endows it with irreplaceable potential in nuclear industries as controlling rod and neutron shield to improve the stability and ensure radiation protection in nuclear power plants[2]. In medicine, ^{10}B is applied for boron neutron capture therapy (BNCT) to treat either surface or deep-seated tumors[3]. Consequently, enriched ^{10}B with high abundance of 80% ~ 85%[4] has been urgently demanded in nuclear industries and radiation therapy. As a contrast, ^{11}B barely with neutron capture capacity, is widely used as a steel manufacturing additive which endows the steel with excellent radiation resistance and high-temperature resistance for the construction of nuclear reactors. In addition, ^{11}B is a potential thermonuclear fuel due to the release of huge energy in thermonuclear reaction[5]. Therefore, the development of techniques for efficient boron isotopic separation has always been a challenge for their individual applications.

To separate boron isotopes which generally have same chemical and physical properties, various methods have been investigated including chemical exchange distillation[4, 6, 7], laser ablation[8], thermal ionization mass spectrometry[9] and adsorption-based chromatography[10-14], among which chemical exchange distillation is the only technique practically implemented in industrial production. However, the low separation factor (~ 1.03) of chemical exchange distillation leads to high plate number[6, 7], consequently considerable energy consumption for

sufficient enrichment of two isotopes. In addition, the traditional distillation facilities suffer severe corrosion with boron trifluoride as feed, leading to their shortened service life and potential safety concerns. Considering the aforementioned obstacles, improved separation ability and mild operation condition are highly favorable for the development of boron isotopic separation techniques. Mildly operated with boric acid solutions as the feed, adsorption-based chromatography for boron isotopic separation has attracted increasing attention where various adsorbents have been investigated including metal-organic frameworks (MOFs)[15], ion exchange resins[10, 11, 14], clay mineral[12, 13] and magnetic nanoparticles[16]. However, their practical applications remain challenging due to high cost of materials, low separation factor as well as complex column packing of understudied materials.

Our previous researches have reported the so far highest boron isotopic separation factor through the newly-discovered interactions between boric acid and the metal sites of MOF materials[15]. Inspired by these results, the easy-prepared magnetic magnetite nanoparticles (MMN) with abundant metal sites was further investigated with remarkable separation factor (1.332) compared with other boron adsorbents and traditional chemical exchange distillation (~ 1.03)[16]. However, extremely high column pressure resulted from the nanosized MMN packing in the chromatographic column became an obstacle for industrial applications.

In response to this situation, we herein developed a novel boron adsorbent (Fe_3O_4@Resin) where nanosized MMNs were synthesized on the substrate, strongly acidic cation (SAC) exchange resin with millimeter-level particle size, stable structure, and high cation exchange capacity. Prior to the co-precipitation, ferrous and/or ferric ions have been

introduced into the commercially available resin functionalized with sulfonic acid groups. Boron adsorption and isotopic separation performance on Fe_3O_4@Resin were investigated including the effect of *p*H, adsorption kinetics and isotherms, dynamic column breakthrough. The reliability of Fe_3O_4@Resin for industrially chromatographic separation of boron isotopes was further proved by the computational simulation with the Chromatography model of Aspen software. The column operation parameters were further optimized by Box-Behnken design (BBD) and reusability performance of Fe_3O_4@Resin was also evaluated. All results demonstrated that Fe_3O_4@Resin reported in this paper can provide an efficient way for industrial boron isotopic separation.

2. EXPERIMENTAL SECTION

2.1. Chemicals

The strongly acidic cation exchange resin D001 (D001 resin hereafter) used as the substrate is commercially available from Nankai Hecheng S&T Company, China, the properties of which were summarized in Table S1. Reagents in this research were used of analytical-grade without further purification. $FeCl_2 \cdot 4H_2O$ (99 wt%), $FeCl_3 \cdot 6H_2O$ (99 wt%), ammonia aqueous solution (25 wt%) were pursed from Shanghai Macklin Biochemical Co., Ltd, China. Hydrochloric acid (36 wt%, Tianjin Jiangtian Chemical Technology Co., Ltd, China) and sodium hydroxide (99 wt%, Tianjin Yuanli Chemical Technology Co., Ltd, China) were applied to adjust the *p*H of boric acid solutions. Hydrochloric acid (0.01 $mol \cdot L^{-1}$, Tianjin Jiangtian Chemical Technology Co., Ltd, China) and deionized water (Tianjin Yuanli Chemical Technology Co., Ltd, China) was employed for the preparation of eluent. Boric

acid (Tianjin Yuanli Chemical Technology Co., Ltd, China) was dissolved in deionized water to prepare boron aqueous solutions. All the obtained solutions were stored in polyethene containers instead of glassware in case of the interference of boron from the glassware.

2.2. Preparation of Fe_3O_4@Resin

2.2.1. Pretreatment of the D001 resin

Prior to the synthesis of Fe_3O_4@Resin composite, D001 resin was pretreated to prepare for the exchange of protons with Fe^{2+} and Fe^{3+} ions. Specifically, the D001 resin (40 mL) which has been washed with deionized water for 3 times, was added into the prepared hydrochloric acid solution (4 wt%, 100 mL) in a three-neck round bottom flask. After being stirred for 12 h, the resin was rinsed with deionized water until the *p*H of the eluent was neutral. Then, the resin was added into the prepared sodium hydroxide aqueous solution (4 wt %, 100 mL). After 12 hours' stirring, the resin was rinsed to neutral again with deionized water and added into hydrochloric acid solution (4 wt%, 200 mL). After 2 hours' stirring, the resin was rinsed to neutral with deionized water for another time and was ready for the synthesis of Fe_3O_4@Resin composites in the next step.

2.2.2. Synthesis of Fe_3O_4@Resin composites

Fe^{2+} and Fe^{3+} loading by cation exchange

The Fe_3O_4@Resin composites was synthesized with the prepared Fe^{2+} and Fe^{3+} loaded D001 resins based on the co-precipitation method reported in our previous research[16]. To evaluate the effect of cation exchange, three different cation exchange protocols were investigated in this study and three Fe_3O_4@Resin composites were obtained accordingly.

Fe_3O_4@Resin-1

In a one-liter three-neck round bottom flask, pre-treated D001 resin (40 mL) and $FeCl_3 \cdot 6H_2O$ (8.1 g) were added into 540 mL deionized water and the mixture was stirred for 12 h to complete the cation exchange between Fe^{3+} and H^+ under N_2 atmosphere. After $FeCl_2 \cdot 4H_2O$ (3.9 g) was added and completely dissolved in the mixture, ammonia aqueous solution (60 mL) was slowly added to adjust the *p*H to 8 for co-precipitation which was carried out under N_2 atmosphere for 1 h. The obtained Fe_3O_4@Resin-1 particles were separated by sedimentation and washed with ethanol and deionized water for 3 times,

respectively. Prior to the characterization, the obtained Fe_3O_4@Resin-1 composite was dried under vacuum for 10 h at 40 °C.

Fe_3O_4@Resin-2

In a one-liter three-neck round bottom flask, pre-treated D001 resin (40 mL) and $FeCl_2 \cdot 4H_2O$ (3.9 g) were added into 540 mL deionized water and the mixture was stirred for 12 h to achieve the cation exchange between Fe^{2+} and H^+ under N_2 atmosphere. After $FeCl_3 \cdot 6H_2O$ (8.1 g) was added and completely dissolved in the mixture, ammonia aqueous solution (60 mL) was slowly added to adjust the *p*H to 8 for co-precipitation which was carried out under N_2 atmosphere for 1 h. The obtained Fe_3O_4@Resin-2 particles were separated by sedimentation and washed with ethanol and deionized water for 3 times, respectively. Prior to the characterization, the obtained Fe_3O_4@Resin-2 composite was dried under vacuum for 10 h at 40 °C.

Fe_3O_4@Resin-3

In a one-liter three-neck round bottom flask, pre-treated D001 resin (40 mL) and $FeCl_2 \cdot 4H_2O$ (3.9 g), $FeCl_3 \cdot 6H_2O$ (8.1 g) were added into 540 mL deionized water and the mixture was stirred for 12 h to achieve the cation exchange between Fe^{2+}, Fe^{3+} and H^+ under N_2 atmosphere. Ammonia aqueous solution (60 mL) was slowly added to adjust the *p*H to 8 for co-precipitation which was carried out under N_2 atmosphere for 1 h. The obtained Fe_3O_4@Resin-3 particles were separated by sedimentation and washed with ethanol and deionized water for 3 times, respectively. Prior to the characterization, the obtained Fe_3O_4@Resin-3 composite was dried under vacuum for 10 h at 40 °C.

Three obtained Fe_3O_4@Resin composites were sieved (24 ~ 32 mesh) with uniform sizes of 0.56 ~ 0.8 mm diameter. In addition, nanosized Fe_3O_4 particles were synthesized according to our previous research for the comparison with Fe_3O_4@Resin composites.

2.3. Characterization

The crystallinity of Fe_3O_4@Resin composites, Fe_3O_4 nanoparticles and D001 resin were assessed by X-ray diffraction (XRD) spectroscopy equipped with anode of Cu (Bruker, λ_{Ka} = 1.5406 Å, Germany) with 2θ angle ranging from 10° to 70°. The morphology of Fe_3O_4@Resin composites and D001 resin was observed via scanning electron microscopy

(SEM, S-4800, Hitachi, Japan) operated at 3.0 KV. Infrared spectra of Fe_3O_4@Resin-1, D001 resin and Fe_3O_4 nanoparticles were recorded from 4000 to 400 cm^{-1} using attenuated total reflection Fourier transform infrared spectroscopy (FT-IR, Spectrum 100, PerkinElmer, USA). Thermogravimetric analyses (TGA, STA449F5, Netzsch, Germany) were obtained through heating the samples from 25 °C to 800 °C at a rate of 10 °C/min under air atmosphere. Boron concentration in the aqueous solutions was tested by inductively coupled plasma-optical emission spectroscopy (ICP-OES, Optima 8000, PerkinElmer, USA). Inductively coupled plasma mass spectrometry (ICP-MS, X Series II, Thermo Electron Corporation, USA) was applied to determine boron isotopic abundance. The internal porosity of Fe_3O_4@Resin-1 was determined by mercury intrusion porosimetry (MIP, Poromaster GT-60, Quantachromre, USA).

2.4. Boron adsorption and isotopic separation

2.4.1. Batch adsorption experiments

Prior to adsorption, the Fe_3O_4@Resin composites were activated under vacuum at 60 °C for 10 h. In order to determine the boron adsorption capacity of the adsorbents, batch adsorption experiments were performed with the adsorbent dosage of 1 g per 20 mL boron aqueous solution (7.567 $g \cdot L^{-1}$, *p*H = 7) in a 50 mL centrifuge tube which was shaken in a thermostatic shaker at 25 °C for 24 h. According to our previous research, Fe_3O_4 nanoparticles achieved the highest adsorption capacity at *p*H = 7 and 45 °C[16]. After removing the adsorbents from the mixture, the solutions were tested for boron concentration where Fe_3O_4@Resin-1 achieved the highest capacity and was further studied in the following experiments.

2.4.2. Effect of *p*H on boron isotopic separation

The *p*H dependence of Fe_3O_4@Resin composites on boron adsorption and isotopic separation capacity were investigated by adjusting the *p*H of the boron solutions from 2 to 11 with hydrochloric acid or sodium hydroxide solutions (1 $mol \cdot L^{-1}$). Activated Fe_3O_4@Resin-1 composite (1 g) was added to prepared boron solutions (5.405 $g \cdot L^{-1}$, 20 mL) with specific *p*Hs and the mixtures were shaken at 25 °C for 24 h. Boron concentration, isotopic abundance and *p*H of residual solutions were tested while the adsorption completed. The best performance was achieved at *p*H = 7 which was kept in the following studies.

2.4.3. Adsorption kinetics

For adsorption kinetic studies, in order to avoid disturbing the system, nine parallel centrifuge tubes containing 1 g activated Fe_3O_4@Resin-1 and 20 mL boron aqueous solution (5.405 $g \cdot L^{-1}$, *p*H = 7), were simultaneously shaken at 25 °C for 24 h. At different time intervals, 1 mL supernatant was sampled from a different centrifuge tube for boron concentration measurement using ICP-OES.

2.4.4. Adsorption isotherms

The adsorption isotherms study was conducted in 50 mL centrifuge tubes with 1 g activated Fe_3O_4@Resin-1 composite and 20 mL boron aqueous solution with varied initial concentrations ranging from 0.5405 to 7.567 $g \cdot L^{-1}$ (*p*H = 7). All the tubes were shaken at 25 °C for 24 h and the residual boron concentrations and isotopic abundances were determined by ICP-OES and ICP-MS, respectively. Reproducibility of adsorption kinetics and isotherms was investigated by repeating above-mentioned experiments for three times. The averaged values were used to fit kinetic and isotherm models.

2.5. Dynamic column experiments

The dynamic column experiment was carried out in a stainless column with a length of 25 cm and a diameter of 2.2 cm. Fe_3O_4@Resin-1 particles (58.81 g) were packed into the

chromatographic column uniformly where uracil solution (3 mL 0.3 g/L) as an inert tracer was injected and the effluent was monitored at regular time intervals to determine the retention time of the packed column.

To obtain the breakthrough curves of boron and two isotopes in the Fe_3O_4@Resin-1 packed column, boron solution (5.405 $g \cdot L^{-1}$, *p*H=7) was pumped into the chromatographic column with constant flow rate Q of 5 $mL \cdot min^{-1}$ at 25 °C. The effluent was sampled continuously at regular time intervals, and further tested for boron concentration and isotopic abundance by ICP-OES and ICP-MS, respectively.

2.6. Recycling

The exhausted Fe_3O_4@Resin-1 composite packed in the chromatographic column was regenerated by 0.01 $mol \cdot L^{-1}$ hydrochloric acid with a flow rate of 5 $mL \cdot min^{-1}$ for 1.5 h, then washed with deionized water until the effluent was neutral. This adsorption/regeneration process was repeated five times to determine the reusability of Fe_3O_4@Resin-1 for boron isotopic separation.

3. MODELS FOR ADSORPTION

3.1. Kinetic models

Intraparticle diffusion model is used to analyze the rate-controlling step of adsorption process[17], which is shown as Eq. (1):

$$Q_t = k_i t^{0.5} + K \tag{1}$$

where Q_t ($mg \cdot g^{-1}$) is the boron adsorption capacity at time t (h); k_i ($mg \cdot g^{-1} \cdot h^{-0.5}$) is the diffusion rate constant and K is the intercept of the curves.

The pseudo-second order model is based on the assumption of chemisorption[18] and defined as the following Eq. (2):

$$\frac{t}{Q_t} = \frac{1}{k_2 Q_e^2} + \frac{1}{Q_e} t \tag{2}$$

where k_2 ($g \cdot mg^{-1} \cdot h^{-1}$) is the rate constant of pseudo-second order adsorption; Q_e ($mg \cdot g^{-1}$) and Q_t ($mg \cdot g^{-1}$) are the boron adsorption capacity at equilibrium and at time t (h).

3.2. Isotherm models

Henry isotherm model assumes that adsorption capacity is proportional to the concentration of the adsorbate[19] and is defined as Eq. (3):

$$Q_e = K_H C_e \tag{3}$$

where Q_e ($mg \cdot g^{-1}$) and C_e ($g \cdot L^{-1}$) are the boron adsorption capacity and boron concentration of solution at equilibrium; K_H ($mL \cdot g^{-1}$) is Henry constant.

The assumption of Langmuir isotherm model is that each adsorptive site can be only occupied in a one-on-one manner[20]. The Langmuir model is expressed as Eq. (4):

$$Q_e = \frac{Q_m K_L C_e}{1 + K_L C_e} \tag{4}$$

where Q_e ($mg \cdot g^{-1}$) and C_e ($g \cdot L^{-1}$) are the boron adsorption capacity and boron concentration of the solution at equilibrium; Q_m ($mg \cdot g^{-1}$) is the maximum adsorption capacity; K_L ($L \cdot g^{-1}$) is the Langmuir equilibrium constant.

3.3. Adsorption chromatographic models

The adsorption column model is defined as following equations[14]:

$$\frac{\partial c}{\partial t} + v\frac{\partial c}{\partial z} = D_L\frac{\partial^2 c}{\partial z^2} - \frac{(1-\varepsilon_B)}{\varepsilon_B}\frac{\partial q}{\partial t} \quad (5)$$

$$\frac{\partial q}{\partial t} = MTC(q^* - q) \quad (6)$$

$$q^* = q^*(c) \quad (7)$$

where c ($g \cdot L^{-1}$) is the concentration of the solute in the mobile phase; q ($g \cdot L^{-1}$) represents the concentration of the solute in the fixed phase; v ($cm \cdot min^{-1}$) is the interstitial velocity; ε_B is the bed porosity; MTC (min^{-1}) is the mass transfer coefficient; D_L ($cm^2 \cdot min^{-1}$) is the axial dispersion coefficient; t (min) is the time; z is the distance in the direction of flow; q^* ($mg \cdot g^{-1}$) is the equilibrium adsorption capacity that is defined as a function of liquid concentrations based on adsorption isotherms. Eq. (5) is obtained by mass balance in a chromatography column. A conventional linear driving force (LDF) model with mass transfer coefficient is employed in Eq. (6), which assumes that the adsorption rate is a linear function of the adsorbent loading[21, 22]. In order to obtain the numerical solution of Eq. (5), two initial conditions and two boundary conditions are required.

$$c(t=0,z) = 0 \quad (8)$$

$$q(t=0,z) = 0 \quad (9)$$

$$z = 0 : c(t) = c_0 + \frac{\varepsilon_B D_L}{v}\frac{\partial c}{\partial z} \quad (10)$$

$$z = L : \frac{\partial c}{\partial z} = 0 \quad (11)$$

Several parameters need to be determined before the simulation of boron isotopes separation process on Aspen chromatography. The overall porosity ε and bed porosity ε_B is calculated by Eq. (12, 13):

$$\varepsilon = \frac{t_0 Q}{\frac{\pi}{4} d^2 L} \tag{12}$$

$$\varepsilon_B = \frac{\varepsilon - \varepsilon_P}{1 - \varepsilon_P} \tag{13}$$

where t_0 (min) is the retention time of the column; Q (mL·min^{-1}) is the volumetric flow rate; d (cm) and L (cm) are the diameter and length of the column, respectively; ε_P is the internal porosity of packed particles which is measured by MIP. Superficial velocity v_s (cm·min^{-1}), interstitial velocity v (cm·min^{-1}) and dispersion coefficient E_Z (cm^2·min^{-1}) of the column are defined as follows:

$$v_s = \frac{Q}{A} \tag{14}$$

$$v = \frac{v_s}{\varepsilon_B} \tag{15}$$

$$E_Z = \frac{v d_p}{Pe} \tag{16}$$

$$Pe = \frac{v_s L}{D_L} \tag{17}$$

where A (cm^2) is cross-sectional area of the column; d_p (cm) is the diameter of packed particles; Pe is constant Peclet number calculated by Eq. (17).

3.4. Performance measurement

The separation factor S, adsorption capacity Q_B (g) and annual yield Y (g) of ^{10}B are evaluated for the boron isotopic separation performance of Fe_3O_4@Resin-1 packed chromatographic column, which are defined as follows:

$$S(^{10}B/^{11}B)=[^{10}B/^{11}B]_{adsorbent}/[^{10}B/^{11}B]_{solution} \quad (18)$$

$$Q_B=\frac{Q}{1000}\int_0^{t_b}(c_f-c(t))dt \quad (19)$$

$$Y=\frac{300\times 24\times 60}{t_c}Q_B \quad (20)$$

where $[^{10}B/^{11}B]_{adsorbent}$ ($g\cdot g^{-1}$) is the ratio of ^{10}B to ^{11}B adsorbed on the adsorbent; $[^{10}B/^{11}B]_{solution}$ ($g\cdot g^{-1}$) is the ratio of ^{10}B to ^{11}B in the solution; t_b (min) is the breakthrough time of ^{10}B; c_f and c ($g\cdot L^{-1}$) are the ^{10}B concentration of feed solution and the effluent, respectively; t_c (min) is the time of a cycle including adsorption and regeneration.

3.5. Box-Behnken design (BBD) model

Box-Behnken design (BBD) model has been widely applied to optimize process parameters in scientific research[23]. In this research, Box-Behnken design (BBD) using Design-Expert 12 software was applied for optimization and three independent parameters including feed boron concentration (C), flow rate (Q), the length of column (L) were selected as variables regarding annual yield (Y) of ^{10}B where each variable was investigated at three predetermined levels (Table 1). Thirteen simulated runs were implemented for the following quadratic polynomial model:

$$Y = \beta_0 + \sum \beta_i X_i + \sum \beta_{ii} X_i^2 + \sum \beta_{ij} X_i X_j \quad (21)$$

where Y is the response variable; β_0 is the constant; β_i, β_{ii}, β_{ij} are regression coefficients for linear, quadratic and interaction terms; X_i and X_j are independent variables.

Table 1 Factors and levels of simulation.

Factors	Unit	Symbol	Levels		
			−1	0	1
C	$g \cdot L^{-1}$	X_1	5.405	6.486	7.567
Q	$mL \cdot min^{-1}$	X_2	5	25	45
L	cm	X_3	25	35	45

4. RESULTS AND DISCUSSION

4.1. Characterization of Fe_3O_4@Resin composites

With the exchange of cations and their co-precipitation on the surface of the D001 resin, three Fe_3O_4@Resin composites were synthesized under different procedures and comprehensively characterized through various techniques including XRD, SEM, FT-IR and TGA. The XRD patterns of three Fe_3O_4@Resin composites were compared to those of as-synthesized Fe_3O_4 nanoparticles, the D001 resin and the simulated pattern of Fe_3O_4 (Figure 1, Table S2). Highly consistent with the simulated and experimental patterns of Fe_3O_4, the characteristic diffraction peaks of Fe_3O_4 in the patterns of Fe_3O_4@Resin composites provided definitive proof for the successful loading of Fe_3O_4 in the resin. Through the half-peak width of the crystal facet (*311*) with the highest diffraction intensity, the crystallite sizes of Fe_3O_4

particles on Fe_3O_4@Resin composites were calculated by Scherer formula[24] to be 13, 28, 31 nm while pristine Fe_3O_4 nanoparticles was calculated to be 13 nm, which indicated the nanoparticle size on Fe_3O_4@Resin-1 constructed with initial exchange of Fe^{3+} ions was much smaller than the other two composites from different synthetic procedures, and its size was very close to that of pristine Fe_3O_4 nanoparticles. The external morphology of obtained Fe_3O_4@Resin composites was observed where a layer of Fe_3O_4 was coated on the surface of the D001 resin bead, leading to less smooth surface (Figure 2). Comparing the SEM images of the three Fe_3O_4@Resin composites, the size of Fe_3O_4 nanoparticles on the surface of Fe_3O_4@Resin-1 composite was smaller and more uniform than those of Fe_3O_4@Resin-2 and Fe_3O_4@Resin-3, which was in good accordance with the XRD observation.

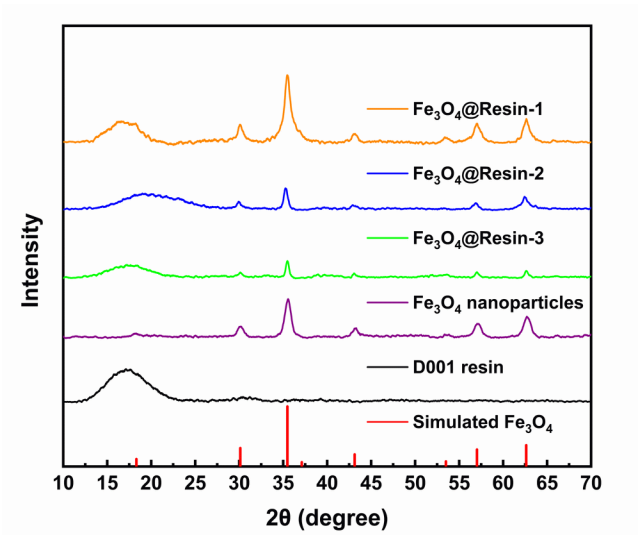

Figure 1. Experimental XRD patterns of Fe_3O_4@Resin composites, as-synthesized Fe_3O_4 nanoparticles, the D001 resin and simulated Fe_3O_4 XRD pattern.

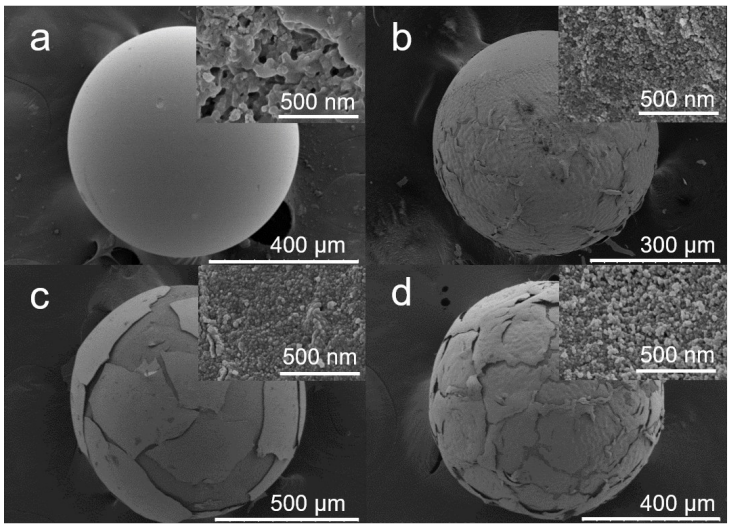

Figure 2. SEM images of (a) the D001 resin; (b) Fe_3O_4@Resin-1 composite; (c) Fe_3O_4@Resin-2 composite; (d) Fe_3O_4@Resin-3 composite.

The FT-IR spectra displayed the characteristic peaks of Fe_3O_4, D001 resin and Fe_3O_4@Resin-1 (Figure 3). The adsorption peak at 586 cm^{-1} corresponding to Fe−O stretching vibration in the FT-IR spectrum of Fe_3O_4@Resin-1 further demonstrated the loading of Fe_3O_4 on the resin while similar spectrum with D001 resin indicated its resin skeleton. The peak at 3176 cm^{-1} of Fe_3O_4@Resin-1 could be attributed to the residual ammonium ion after synthesis. The thermal stability of Fe_3O_4@Resin-1 were evaluated and compared with parent D001 resin where the weight loss lower than 200 °C was mainly due to the elimination of adsorbed water and the weight loss at > 200 °C corresponded to the decarboxylation and carbonization of polymer chains[25] (Figure 4). The weight loss of Fe_3O_4@Resin-1 reached equilibrium at 700 °C where the resin decomposed into inorganic ashes and Fe_3O_4 was oxidized into Fe_2O_3. The weight ratio of Fe_3O_4 nanoparticles in Fe_3O_4@Resin-1 was calculated to be around 8.1%.

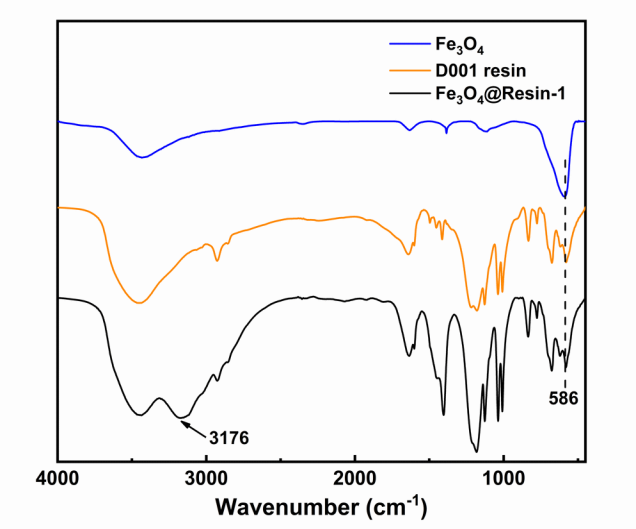

Figure 3. FT-IR spectra of Fe_3O_4@Resin-1, the D001 resin and Fe_3O_4 nanoparticles.

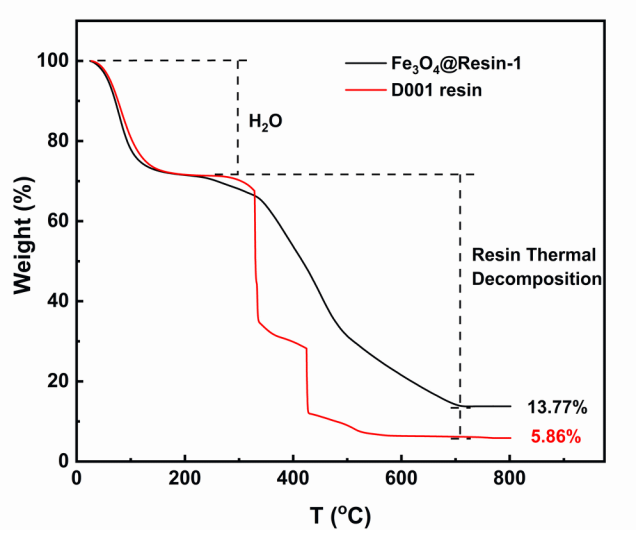

Figure 4. Thermogravimetric curve of Fe_3O_4@Resin-1 and the D001 resin.

4.2. Batch experiment results

The boron adsorption capacity of three Fe_3O_4@Resin composites and the parent D001 resin was determined by the batch adsorption experiments to be 3.213, 2.940, 2.727 and 0 $mg \cdot g^{-1}$, indicating that boron adsorption only happened on Fe_3O_4 in the Fe_3O_4@Resin composites and the Fe_3O_4@Resin-1 composite exhibited the best performance due to its

smaller particle size and more uniform morphology. According to TGA results, it could be calculated that the adsorption capacity of Fe_3O_4 on Fe_3O_4@Resin-1 composite was 39.66 $mg \cdot g^{-1}$, which was comparable with our previous research with pristine Fe_3O_4 as adsorbents (49.54 $mg \cdot g^{-1}$)[16]. The reduced capacity could be attributed to that partial active sites of the loaded Fe_3O_4 was blocked by the resin.

4.3. Effect of *p*H on boron adsorption

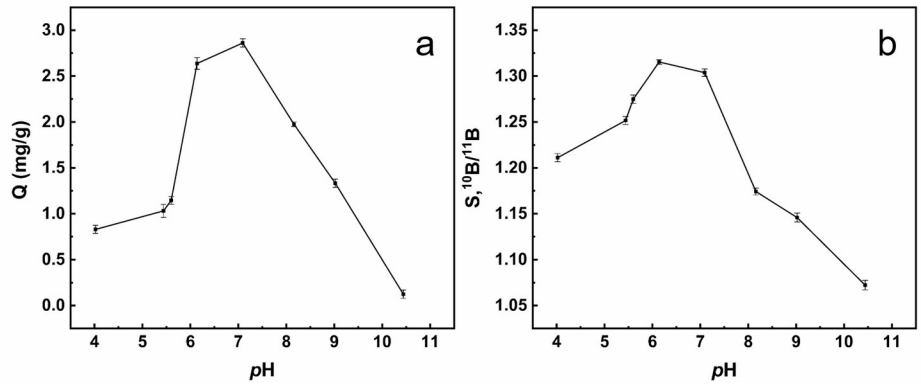

Figure 5. Effect of *p*H on (a) boron adsorption capacity and (b) isotopic separation factor.

Boric acid in aqueous solution mainly exists in two forms, $B(OH)_3$ and $B(OH)_4^-$ at different *p*H ranges where the concentration of $B(OH)_3$ decreased while improved $B(OH)_4^-$ concentration was observed with elevated *p*H[26]. Additionally, diverse surface charges of Fe_3O_4 at different *p*Hs could potentially influence the adsorption behavior[27-29]. Along with boron adsorption on the Fe_3O_4@Resin-1 composite, the *p*H of the boron aqueous solution plays a critical role in the boron species distribution and surface charges of the adsorbents, consequent adsorption capacity and isotopic separation factor. To evaluate the influence of *p*H, various *p*H conditions were investigated where the adsorption capacity and isotopic

separation factor reached their maximum of 2.869 $mg \cdot g^{-1}$ at *p*H = 7 and 1.315 at *p*H = 6, respectively (Figure 5). The observed trend was in good accordance with previous reported Fe_3O_4, and a *p*H of 7 was fixed in the following research. Besides, repeating experiments for three times showed favorable reproducibility of adsorption performance.

4.4. Adsorption kinetics

Time-dependent boron adsorption capacity on Fe_3O_4@Resin-1 composite was obtained through kinetic studies. Adsorption capacity increased rapidly in the first half hour, and reached the adsorption equilibrium in the next half hour (Figure 6a). The intraparticle diffusion and pseudo-second order kinetic models were employed for adsorption kinetic analysis while the pseudo-first order model cannot fit the data well.

Related kinetic parameters of two models were summarized in Table 2. The kinetic data was fitted with intraparticle diffusion model with three linear portions, of which the first portion did not go through the zero point, indicating that a rapid adsorption occurs within a short period of time and the intraparticle diffusion was not the only rate-controlling step[17, 30] (Figure 6b). The initial fast process was followed by a much slower second kinetic regime and a third portion with nearly zero slope, indicating the equilibrium state was attained[20, 31]. With pseudo-second order model, the plot of t/Q_t against t had higher correlation coefficient (R^2) and the experimental adsorption capacity Q_e (2.832 $mg \cdot g^{-1}$) was very close to the calculated values, indicating that chemisorption process could be the rate-controlling step[18] (Figure 6c).

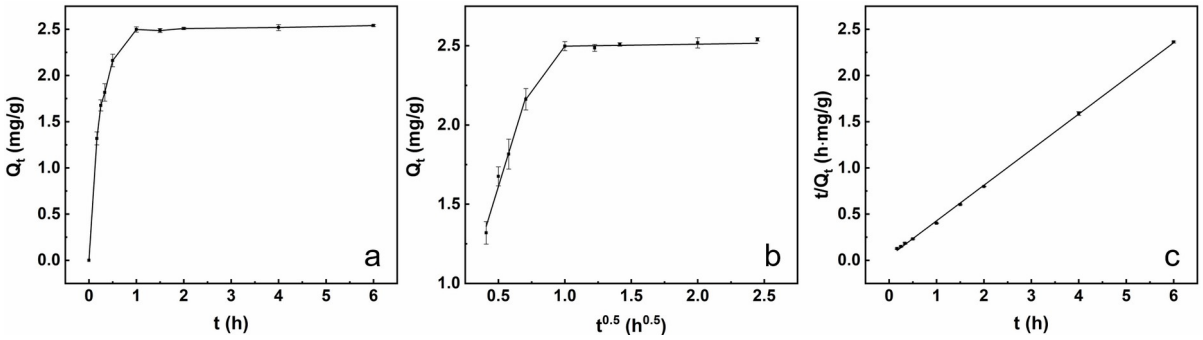

Figure 6. (a) Time-dependent boron adsorption capacity on Fe_3O_4@Resin-1 composite; (b) Intraparticle diffusion and (c) pseudo-second order kinetics of boron adsorption on Fe_3O_4@Resin-1 composite.

Table 2 Boron adsorption kinetic parameters of different models on Fe_3O_4@Resin-1 composite.

	Intraparticle diffusion model			Pseudo second-order model		
	K	k_i $mg \cdot g^{-1} \cdot h^{-0.5}$	R^2	k_2 $g \cdot mg^{-1} \cdot h^{-1}$	Q_e *(cal.)* $mg \cdot g^{-1}$	R^2
First portion	0.2434	2.7357	0.9747			
Second portion	1.3530	1.1441	0.9999	3.597	2.595	0.9995
Third portion	2.4572	0.0327	0.8333			

4.5. Adsorption isotherms

Increased adsorption capacities of total boron, ^{11}B and ^{10}B on Fe_3O_4@Resin-1 were observed with improved initial boron concentration at 25 °C from the adsorption isotherm experiments (Figure 7a), which was analyzed to investigate the boron adsorptive behaviors (Figure 7b, c, Table 3). Fitting curves by the Langmuir model implied a better description of the experimental results than the Henry model, which demonstrated that the boron adsorption on Fe_3O_4@Resin-1 could be a monolayer chemisorption process on the homogenous

surface[32]. Relevant parameters of Langmuir model were directly employed for following dynamic simulation by Aspen Chromatography.

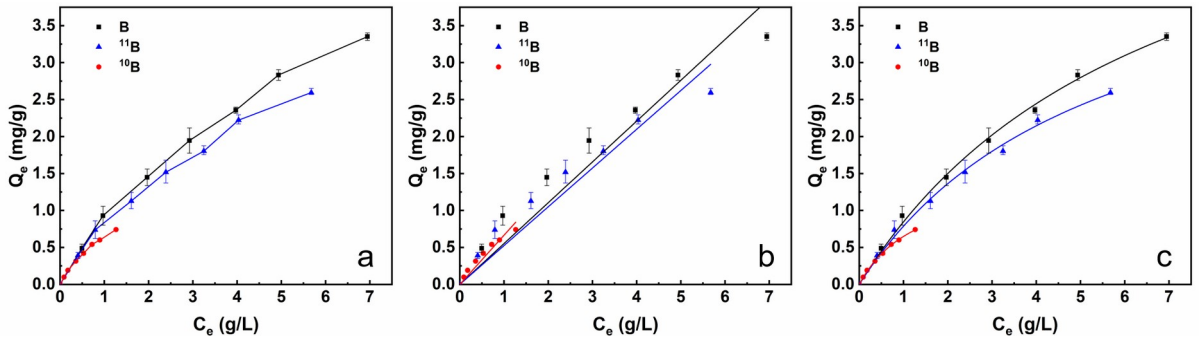

Figure 7. (a) Adsorption isotherms and isotherm fitting curves of boron, boron-11 and boron-10 on Fe_3O_4@Resin-1 composite with (b) the Henry model and (c) the Langmuir model.

Table 3 Boron adsorption parameters of different isotherm models on Fe_3O_4@Resin-1 composite.

Adsorbates	Henry model		Langmuir model		
	K_H	R^2	Q_m	K_L	R^2
	$mL \cdot g^{-1}$		$mg \cdot g^{-1}$	$L \cdot g^{-1}$	
B	0.5520	0.9743	6.612	0.1466	0.9970
^{11}B	0.5244	0.9730	5.053	0.1844	0.9950
^{10}B	0.6647	0.9770	1.525	0.7392	0.9987

4.6. Dynamic column experiments

Using Fe_3O_4@Resin-1 packed chromatographic column, the experimental breakthrough curves of ^{10}B and ^{11}B in the effluent were recorded with time (Figure 8).

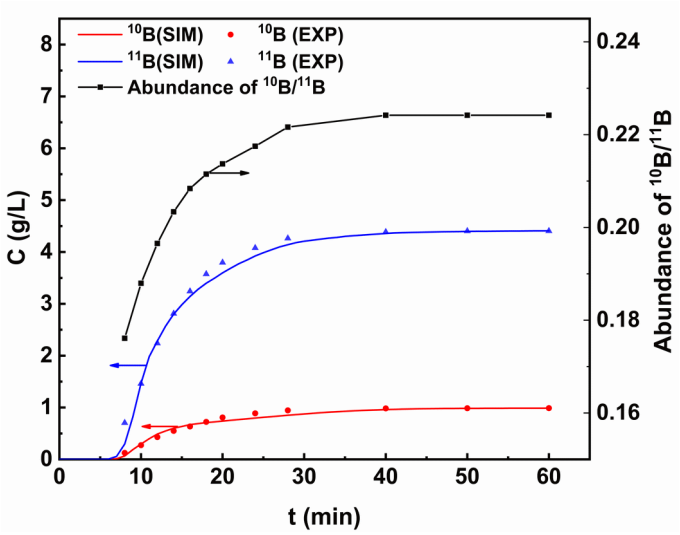

Figure 8. Breakthrough curves of ^{10}B and ^{11}B on the dynamic column experiment. Points: experimental data. Solid lines: simulation data by Aspen Chromatography.

The boron isotopic abundance of the effluent was 0.176 for initial sampling which was much less than the abundance of the feed boron solution (0.224), gradually reached the same as the feed. The breakthrough time of ^{10}B and ^{11}B were 35 min and 30 min, and their adsorption amount was calculated to be 0.03412 g and 0.1274 g, respectively, indicating the higher affinity between Fe_3O_4@Resin-1 and ^{10}B and the enrichment of ^{10}B in chromatographic separation process. The dynamic adsorption capacity for total boron was 2.747 mg·g^{-1} and the separation factor S (^{10}B/^{11}B) was 1.312, basically consistent with the batch adsorption results (2.832 mg·g^{-1}, 1.304). More importantly, the column pressure was below 2 MPa, which is much lower than that (~50 MPa) of a similar-sized column packed with Fe_3O_4 nanoparticles, indicating its feasibility in actual industrial operation. The simulated breakthrough curves by Aspen Chromatography based on Langmuir model matched well with the experimental results for two isotopes (Figure 8, Table 4).

Consequently, Langmuir model was reliable to be employed in the following process optimization.

Table 4 Parameters for separation process simulation on Aspen Chromatography.

Parameters	Value
L (cm)	25
D (cm)	2.2
ε_B	0.349
ε_P	0.272
E_Z ($cm^2 \cdot min^{-1}$)	0.000528
MTC (min^{-1})	0.0810
Q ($mL \cdot min^{-1}$)	5
^{10}B C_f ($g \cdot L^{-1}$)	0.989
^{11}B C_f ($g \cdot L^{-1}$)	4.416
PDE discretization scheme	USD1
The number of nodes	100

4.7. Box-Behnken design (BBD) for process optimization

Thirteen runs designed by BBD for optimizing the operated conditions and corresponding responses calculated by the simulated results in Aspen Chromatography were listed in Table S3. As a result, the relationship between response variable and operating variables was obtained as follows:

$$Y = 29.7264 - 2.9645X_1 + 0.7476X_2 - 0.3226X_3 + 0.0931X_1X_2 + 1.6406X_1X_3 + 0.1056X_2X_3 - 0.1325X_1^2 - 0.0805X_2^2 - 0.0253X_3^2 \quad (22)$$

Table 5 Analysis of variance of the quadratic model.

Source	Sum of Squares	df	Mean Square	F-value	p-value	Significance
Model	1.379×10^5	9	15326.67	163.82	0.0007	Significant
X_1	28344.20	1	28344.20	320.95	0.0004	Significant
X_2	3350.19	1	3350.19	35.81	0.0093	Significant
X_3	1.001×10^5	1	1.001×10^5	1070.33	< 0.0001	Significant
X_1X_2	16.19	1	16.19	0.1731	0.7054	
X_1X_3	1258.06	1	1258.06	13.45	0.0351	Significant
X_2X_3	1783.60	1	1783.60	19.06	0.0222	Significant
X_1^2	0.1010	1	0.1010	0.0006	0.9822	
X_2^2	4362.15	1	4362.15	25.31	0.0151	Significant
X_3^2	26.91	1	26.91	0.1561	0.7192	
Residual	280.68	3	93.56			
Cor Total	1.382×10^5	12				

Analysis of variance (ANOVA) was employed to evaluate the quality of the quadratic model (Table 5). The F-value and P-value (163.82, < 0.001) implied the model was suitable for predicting experimental data in terms of statistical significance. X_1, X_2, X_3, X_1X_3, X_2X_3, X_2^2 were significant model terms ($P < 0.05$) suggesting significant interaction of X_1 and X_3, X_2 and X_3. The predicted R^2 of 0.9678 was in reasonable agreement with the adjusted R^2 of 0.9954, indicating that the quadratic model equation can predict experimental data significantly. According to the model equation, the optimal operating conditions were

obtained as follows: feed boron concentration of 7.567 $g \cdot L^{-1}$, flow rate of 38.57 $mL \cdot min^{-1}$, the length of column of 45 cm for annual yield of ^{10}B of 612 g. With the scale-up of chromatographic column by increasing column diameter to 1 meter and column length to 2 meters, the annual yield of ^{10}B can reach 375 kg which is comparable to the annual yield of only available boron isotope separation technique (chemical exchange distillation).

4.8. Recycling ability

Considering the critical role of reusability of adsorbents in the practical application, five adsorption-desorption cycles were carried out in chromatographic column to evaluate the reusability of Fe_3O_4@Resin-1. The results showed that the adsorption capacity slightly decreased after five cycles (Figure 9), suggesting that Fe_3O_4@Resin-1 is promising to be applied in practice.

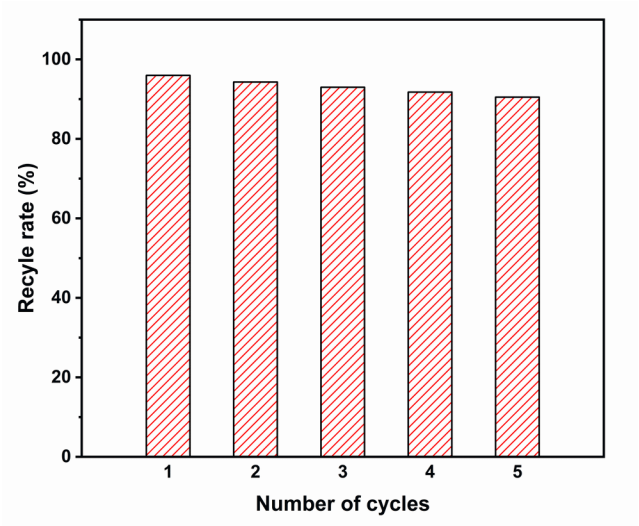

Figure 9. Recycling of Fe_3O_4@Resin-1 on dynamic boron adsorption in five cycles.

5. Conclusions

Three Fe_3O_4@Resin composites were synthesized through ion exchange and co-

precipitated of Fe^{2+} and Fe^{3+} on strong acid ion exchange resin. The as-synthesized Fe_3O_4@Resin composites was comprehensively characterized by XRD, SEM, FT-IR, TGA and evaluated for $^{10}B/^{11}B$ separation, among which Fe_3O_4@Resin-1 constructed with initial exchange of Fe^{3+} ions is the best performer. The boron adsorption and isotopic separation capabilities with Fe_3O_4@Resin-1 were investigated on effect of *p*H, kinetics and isotherms through batch adsorption experiment which can be well described by pseudo-second order kinetics and Langmuir model. A chromatographic column packed with Fe_3O_4@Resin-1 particles was employed for dynamic separation of boron isotopes with a high dynamic separation factor of 1.312 and much lower column pressure than a column packed with Fe_3O_4 nanoparticles. The breakthrough curves of ^{10}B and ^{11}B simulated by Aspen Chromatography were consistent with the experimental data. The column separation performance was further simulated by Aspen Chromatography under different conditions designed by BBD for the optimization of separation process. As a result, the optimal operating conditions were feed boron concentration of 7.567 $g \cdot L^{-1}$, flow rate of 38.57 $mL \cdot min^{-1}$, **column size of 2.2×45 cm (I.D. × length)**, with the highest annual yield of 612 g ^{10}B. Besides, Fe_3O_4@Resin-1 exhibited favorable reusability after five cycles. In summary, excellent dynamic separation factor of boron isotopes, millimeter-level particle size, low cost and favorable reusability empower Fe_3O_4@Resin-1 as a promising adsorbent for enrichment of ^{10}B in industrial application, and this research lays the foundation for the industrial scale-up design and application of boron isotopic separation in the future. However, industrial scale-up and in-depth study of the adsorption mechanism remains a challenge for the future exploration.

Acknowledgments

This project was supported by National Natural Science Foundation of China (No. 22078235), China Postdoctoral Science Foundation (2019M661022) and National Natural Science Foundation of China (No. 22008176).

References

1. **Wang B, Guo X, Bai P. Removal technology of boron dissolved in aqueous solutions – A review. *Colloids and Surfaces A: Physicochemical and Engineering Aspects*. 2014; 444: 338-344.**
2. **Zawisky M, Basturk M, Derntl R, Dubus F, Lehmann E, et al. Non-destructive ^{10}B analysis in neutron transmission experiments. *Applied Radiation and Isotopes.* 2004; 61(4): 517-523.**
3. **Rasouli FS, Masoudi SF. A study on the optimum fast neutron flux for Boron Neutron Capture Therapy of deep-seated tumors. *Applied Radiation and Isotopes*. 2015; 96: 45-51.**
4. **Wu X, Bai P, Guo X, He N. 2,4-Difluoro anisole: a promising complexing agent for boron isotopes separation by chemical exchange reaction and distillation. *Journal of Radioanalytical and Nuclear Chemistry*. 2014; 300(3): 897-902.**
5. **Ivanov VA, Katalnikov SG. Physico-Chemical and Engineering Principles of Boron Isotopes Separation by Using Bf_3–Anisole·Bf_3 system. *Separation Science and Technology*. 2001; 36(8-9): 1737-1768.**
6. **Bai P, Fan K, Guo X, Zhang H. Non-equilibrium mass transfer absorption model for the design of boron isotopes chemical exchange column. *Annals of Nuclear Energy*. 2016; 92: 16-20.**
7. **Abdollahi M, Ahmadi SJ. Application of ideal temperature gradient technology to optimize the chemical exchange and distillation process of boron isotopes separation by $(CH_3)_2O$-BF_3 complex. *Chemical Engineering and Processing: Process***

Intensification. 2014; 76: 26-32.

8. Joseph M, Manoravi P. Boron isotope enrichment in nanosecond pulsed laser-ablation plume. *Applied Physics A: Materials Science and Processing*. 2003; 76(2): 153-156.
9. He M-y, Xiao Y-k, Jin Z-d, Ma Y-q, Xiao J, et al. Accurate and Precise Determination of Boron Isotopic Ratios at Low Concentration by Positive Thermal Ionization Mass Spectrometry Using Static Multicollection of Cs_2BO^{2+} Ions. *Analytical Chemistry*. 2013; 85(13): 6248-6253.
10. Musashi M, Oi T, Matsuo M, Nomura M. Column chromatographic boron isotope separation at 5 and 17 MPa with diluted boric acid solution. *Journal of Chromatography A*. 2008; 1201(1): 48-53.
11. Sharma BK, Rajamani P, Mathur PK. Use of type-II strong base anion exchange resins for ion exchange chromatographic separation of isotopes of boron. *Indian Journal of Chemical Technology*. 1997; 4(6): 308-316.
12. Musashi M, Matsuo M, Oi T, Fujii Y. Chromatographic observation of boron isotopic fractionation between kaolin clay and boron bearing solution: A high pressure experiment. *Geochemical Journal*. 2005; 39(1): 105-111.
13. Musashi M, Matsuo M, Oi T, Nomura M. Chromatographic Study on Boron Isotopic Fractionation at High Pressure. *Journal of Nuclear Science and Technology*. 2006; 43(4): 461-467.
14. Zhang N, Lyu J, Bai P, Guo X. Boron isotopic separation with pyrocatechol-modified resin by chromatography technology: Experiment and numerical

simulation. *Journal of Industrial and Engineering Chemistry*. 2018; 57: 244-253.

15. **Lyu J, Liu H, Zhang J, Zeng Z, Bai P, et al. Metal–organic frameworks (MOFs) as highly efficient agents for boron removal and boron isotope separation. *RSC Advances*. 2017; 7(26): 16022-16026.**
16. **Chen T, Wang Q, Lyu J, Bai P, Guo X. Boron removal and reclamation by magnetic magnetite (Fe_3O_4) nanoparticle: An adsorption and isotopic separation study. *Separation and Purification Technology*. 2020; 231: 115930.**
17. **Vadivelan V, Kumar KV. Equilibrium, kinetics, mechanism, and process design for the sorption of methylene blue onto rice husk. *Journal of Colloid and Interface Science*. 2005; 286(1): 90-100.**
18. **Ho YS, McKay G. Pseudo-second order model for sorption processes. *Process Biochemistry*. 1999; 34(5): 451-465.**
19. **Al-Ghouti MA, Da'ana DA. Guidelines for the use and interpretation of adsorption isotherm models: A review. *Journal of Hazardous Materials*. 2020: 122383.**
20. **Li Q, Fu L, Wang Z, Li A, Shuang C, et al. Synthesis and characterization of a novel magnetic cation exchange resin and its application for efficient removal of Cu^{2+} and Ni^{2+} from aqueous solutions. *Journal of Cleaner Production*. 2017; 165: 801-810.**
21. **Lim Y-I. An optimization strategy for nonlinear simulated moving bed chromatography: Multi-level optimization procedure (MLOP). *Korean Journal of Chemical Engineering*. 2004; 21(4): 836-852.**
22. **Grosfils V. A systematic approach to SMB process model identification from SMB**

process data. *World Congress*. 2005. 2234-2234.

23. **Li C, Zhao C, Ma Y, Chen W, Zheng Y, et al. Optimization of ultrasonic-assisted ultrafiltration process for removing bacterial endotoxin from diammonium glycyrrhizinate using response surface methodology. *Ultrasonics Sonochemistry*. 2020; 68: 105215.**
24. **Si S, Li C, Wang X, Yu D, Peng Q, et al. Magnetic Monodisperse Fe_3O_4 Nanoparticles. *Crystal Growth & Design*. 2005; 5(2): 391-393.**
25. **Li Q, Wang C, Hua M, Shuang C, Li A, et al. High-efficient removal of phthalate esters from aqueous solution with an easily regenerative magnetic resin: Hydrolytic degradation and simultaneous adsorption. *Journal of Cleaner Production*. 2018; 175: 376-383.**
26. **Edzwald JK, Haarhoff J. Seawater pretreatment for reverse osmosis: Chemistry, contaminants, and coagulation. *Water Research*. 2011; 45(17): 5428-5440.**
27. **Chowdhury SR, Yanful EK, Pratt AR. Chemical states in XPS and Raman analysis during removal of Cr(VI) from contaminated water by mixed maghemite–magnetite nanoparticles. *Journal of Hazardous Materials*. 2012; 235-236: 246-256.**
28. **Afkhami A, Moosavi R. Adsorptive removal of Congo red, a carcinogenic textile dye, from aqueous solutions by maghemite nanoparticles. *Journal of Hazardous Materials*. 2010; 174(1): 398-403.**
29. **Wu Y, Chen R, Liu H, Wei Y, Wu D. Feasibility and mechanism of p-nitrophenol decomposition in aqueous dispersions of ferrihydrite and H_2O_2 under irradiation. *Reaction Kinetics, Mechanisms and Catalysis*. 2013; 110(1): 87-99.**

30. **Wu F-C, Tseng R-L, Juang R-S. Initial behavior of intraparticle diffusion model used in the description of adsorption kinetics. *Chemical Engineering Journal*. 2009; 153(1-3): 1-8.**

31. **Brandani S. Kinetics of liquid phase batch adsorption experiments. *Adsorption*. 2020.**

32. **Song W, Gao B, Xu X, Xing L, Han S, et al. Adsorption-desorption behavior of magnetic amine/Fe_3O_4 functionalized biopolymer resin towards anionic dyes from wastewater. *Bioresour Technol*. 2016; 210: 123-30.**